A Physical Model to Determine Snowfall Over Land by Microwave Radiometry

Gail M. Skofronick-Jackson, *Senior Member, IEEE*, Min-Jeong Kim, *Student Member, IEEE*, James A. Weinman, *Senior Member, IEEE*, and Dong-Eon Chang

***Abstract*—Falling snow is an important component of global precipitation in extratropical regions. This paper describes the methodology and results of physically based retrievals of snow falling over land surfaces. Because microwave brightness temperatures emitted by snow-covered surfaces are highly variable, precipitating snow above such surfaces is difficult to observe using window channels that occur at low frequencies ($\nu < 100$ GHz). Furthermore, at frequencies $\nu \leq 37$ GHz, sensitivity to liquid hydrometeors is dominant. These problems are mitigated at high frequencies ($\nu > 100$ GHz) where water vapor screens the surface emission, and sensitivity to frozen hydrometeors is significant. However, the scattering effect of snowfall in the atmosphere at those higher frequencies is also impacted by water vapor in the upper atmosphere. The theory of scattering by randomly oriented dry snow particles at high microwave frequencies appears to be better described by regarding snow as a concatenation of "equivalent" ice spheres rather than as a sphere with the effective dielectric constant of an air–ice mixture. An equivalent sphere snow scattering model was validated against high-frequency attenuation measurements. Satellite-based high-frequency observations from an Advanced Microwave Sounding Unit (AMSU-B) instrument during the March 5–6, 2001 New England blizzard were used to retrieve snowfall over land. Vertical distributions of snow, temperature, and relative humidity profiles were derived from the Mesoscale Model (MM5) cloud model. Those data were applied and modified in a radiative transfer model that derived brightness temperatures consistent with the AMSU-B observations. The retrieved snowfall distribution was validated with radar reflectivity measurements obtained from a ground-based radar network.**

***Index Terms*—Electromagnetic scattering, estimation, millimeter-wave radiometry, remote sensing, satellite, snow.**

I. Introduction

MEASUREMENT of global precipitation is one of the goals of climate studies. Although most global precipitation occurs as rainfall, snowfall plays a significant role in the extratropical hydrological cycle. Snow, falling early in winter, can retard freezing of the underlying soil, thereby allowing subsequent melt water to penetrate the ground. Conversely, if the ground freezes because snow falls late in winter, flooding may ensue from run-off during the spring thaw. Snow also serves as a reservoir of water that can be released later in the year to support agriculture and hydroelectric power generation. Snowstorms can also be hazardous for transportation and other economic activities. One of the most important challenges for future satellites is to detect snowstorms from space. This paper presents a physical model of radiation at millimeter-wave frequencies that seeks to infer snowfall rates over land by taking advantage of water vapor screening to obscure the underlying snow-covered surface.

Midlatitude precipitation occurs in a wide variety of forms from snow to drizzle to rain and to hail [1]. Storm types include multicell and supercell thunderstorms, extratropical cyclones, and hurricanes. The well-developed techniques to study tropical precipitation, using frequencies ≤ 90 GHz, addressed rain occurring in nearly moist adiabatic environments. Extratropical cyclones are a completely different setting for precipitation than any type of tropical storm. Broad zones of frontal lifting produce broad sheets of clouds and precipitation that are mostly though not completely stratiform. These stratiform precipitation regions are similar microphysically to the stratiform regions of tropical mesoscale convective systems. However, the generally cooler conditions often produce a melting layer that is near the earth's surface. Under the coldest conditions, the precipitation reaches the surface as snow.

Most spaceborne remote sensing of snow has addressed the measurement of snow accumulation on the ground (see [2]). Snow within the atmosphere has mainly been derived from microwave radiometry over oceanic regions where the measurements were not affected by snow accumulated on the ground [3]–[6]. Furthermore, most of the snow considered in the above studies are frozen particles above the melting layer or anvil ice clouds, not snow falling at the surface. Because snow accumulation on land affects the emission properties of the surface, the measurement of snowfall within the atmosphere has been difficult with radiometers that operate at frequencies less than 100 GHz where the atmosphere is relatively transparent, and the sensitivity to frozen particles is lower than at higher frequencies. Snow falling over land has been derived from the brightness temperatures at frequencies where absorption occurs using empirical relationships by Kongoli *et al.* [7] and by Chen and Staelin [8]. Although such empirical relationships are operationally useful, physical models are needed to understand how the retrieved snowfall depends on the various ground and atmospheric factors that affect the measured brightness temperatures.

Manuscript received June 27, 2003; revised December 22, 2003.

G. M. Skofronick-Jackson is with the Microwave Sensors Branch, NASA Goddard Space Flight Center, Greenbelt, MD 20771 USA (e-mail: gailsjackson@ieee.org).

M.-J. Kim is with the Department of Atmospheric Science, University of Washington, Seattle, WA 98195 USA.

J. A. Weinman was with the Microwave Sensors Branch, NASA Goddard Space Flight Center, Greenbelt, MD 20771 USA. He is now with the Department of Atmospheric Science, University of Washington, Seattle, WA 98195 USA.

D.-E. Chang was with the Microwave Sensors Branch, NASA Goddard Space Flight Center, Greenbelt, MD 20771 USA. He is now with the Forecast Research Laboratory, Meteorological Research Institute, Korea Meteorological Administration, Seoul 156-720, Korea.

Digital Object Identifier 10.1109/TGRS.2004.825585

To our knowledge, this is the first retrieval of snow falling over land based on a physical model.

The Advanced Microwave Sounding Units (AMSU-B) radiometers on the National Oceanic and Atmospheric Administration (NOAA) 15, 16, 17 spacecraft [9] have the channel set and resolution to resolve locally intense precipitation. The AMSU-B has a nominal 15-km-diameter footprint at nadir and provides observations at 89, 150, and 183 ± 1, ± 3, and ± 7 GHz. These channels are sensitive to both the water vapor (for surface screening) and the snow particles. The AMSU-B radiometer on NOAA 15 initially encountered radio frequency interference from onboard transmitters that were ultimately shut down in the autumn of 1999. Software fixes were encoded in late 1999 so that reliable spaceborne data at frequencies greater 100 GHz were available by January 2000. The NOAA 16 and 17 did not have problems with radio frequency interference. This paper presents a physical model that was used to derive snowfall over land from AMSU-B observations.

II. Case Study

The blizzard of March 5–6, 2001 presented a unique opportunity to observe intense snowfall over land. That blizzard was one of the more intense snow storms of the season, depositing on the order of 50 cm of snow on much of Vermont, New Hampshire, and northeastern New York State with several stations reporting that 75 cm were deposited for the day. Both the NOAA 15 and 16 satellites observed this blizzard (NOAA 17 was launched in June 2002). However, the best spatial and temporal coverage between available ground radar data and AMSU-B data was at 23:00 UTC with the NOAA 15 AMSU-B observations.

A. Radar Data

Fig. 1(a) shows a composite of the National Weather Service (NWS) operational weather radar reflectivity Z_{eff} (millimeters to the sixth power per cubic meter) obtained from several ground stations over the Northeastern United States on March 5, 2001 at 23:00 UTC. Note that the limited range of the radar data does not extend far over the ocean area [Fig. 1(a)]. The snowfall was greatest over Connecticut, Maine, Vermont, and New Hampshire. This composite of Z_{eff} is based on whichever of the lowest four antenna elevations yield the highest reflectivity. At ranges beyond 50 km from the radar, those elevation angles are usually 0.5°. The heights at which those reflectivities are measured varies with distance from the particular radar, falling between 0.5 and $\sim$ 2.5 km. Although the NWS operational radar data have well-known limitations, in the absence of a preplanned field observation campaign, they provide readily available observations to compare to snowfall derived from microwave brightness temperatures.

The radar reflectivity data were smoothed with a 16×16 km template to match the finest spatial resolution of the AMSU-B channels. The center points of the smoothed radar data matched those of the AMSU-B latitude and longitude center points for each footprint. The NWS radar reflectivity resolution is very fine, however, its latitude and longitude mapping was not precise (offsets by no more than 0.1°). Averaging the NWS image to the AMSU-B resolution tended to smooth any effects of location mismatch. The maximum reflectivity in the smoothed radar reflectivity data over the land is $\sim$37 dBZ. Depending on the relationships used to convert from logarithmic power (dBZ) to rainfall rate and then from rainfall rate to snowfall rate, this reflectivity can correspond to snowfall rates between 40 and 125 mm $\cdot$ h^{-1}, with the smaller numbers for wet snow that compresses the snow pack.

B. Microwave Data From AMSU-B

Brightness temperatures Tb_{150} measured by the 150-GHz channel of the NOAA 15 AMSU-B, at 23:02 UTC March 5, 2001, are shown in Fig. 1(b). Note the cold brightness temperatures (< 240 K) in the blizzard region over Vermont and New Hampshire (near 42° to 44°N, 71° to 74°W), and the absence of contrast in surface features such as the Gulf of St. Lawrence (near 47°N, 72°W) and the Great Lakes (near 44°N, 77°W). The 150-GHz brightness temperature distribution is similar to the radar Z_{eff} distribution shown in Fig. 1(a). Fig. 1(c)–(f) shows the distributions of the 89- and 183 $\pm$ 7-, $\pm$3-, $\pm$1-GHz brightness temperatures, (Tb_{89}, $Tb_{183\pm7}$, $Tb_{183\pm3}$, and $Tb_{183\pm1}$, respectively) measured from AMSU-B at 23:02 UTC on March 5, 2001. It is possible that some of the cold Tb_{89} values scattered over Canada may have been caused by accumulated antecedent snow. At 89 GHz, it is difficult to distinguish snow in the atmosphere from snow and other features on the ground. Note that the Great Lakes and the St. Lawrence River, that are evident in Fig. 1(c), are screened by water vapor in the 183-GHz channels in Fig. 1(d)–(f). The 183 $\pm$ 7-, $\pm$3-, $\pm$1-GHz water vapor channels are increasingly sensitive to the water vapor in the cloud profile. At 183 $\pm$ 1 GHz, closest to the water vapor line, saturation with respect to the water vapor occurs quickly near the cold top of the cloud. At 183 $\pm$ 7 GHz, sensitivity to water vapor is decreased and this frequency can probe into the deep snow layers. Although brightness temperatures are more affected by the water vapor profile, evidence of the snow still persists in the 183 $\pm$ 3-GHz channel. The $Tb_{183\pm1}$ measurement reveals little indication of the blizzard, being mainly responsive to water vapor at altitudes above the heaviest precipitation. It should be noted that the core of the snowstorm is at about 35° from nadir in the AMSU-B scanning pattern. A 35° angle translates to about a 15×25 km footprint. The change in footprint size as a function of viewing angle can be seen in the change in the size of pixel rectangles in Fig. 1(b)–(f).

III. Snow Retrieval Method

This paper seeks to derive characteristics of snow whose electromagnetic properties are consistent with microwave brightness temperatures at several frequencies provided by the AMSU-B sensors. Brightness temperatures are computed from an Eddington approximation [10] of the second kind. That radiative transfer model employs information generated from a six parameter model of the atmosphere associated with snow storms. Three of the six parameters are allowed to vary to generate different snow cloud and surface conditions, the other three parameters are set to fixed values based on statistics from a cloud resolving model and external measurements. It is

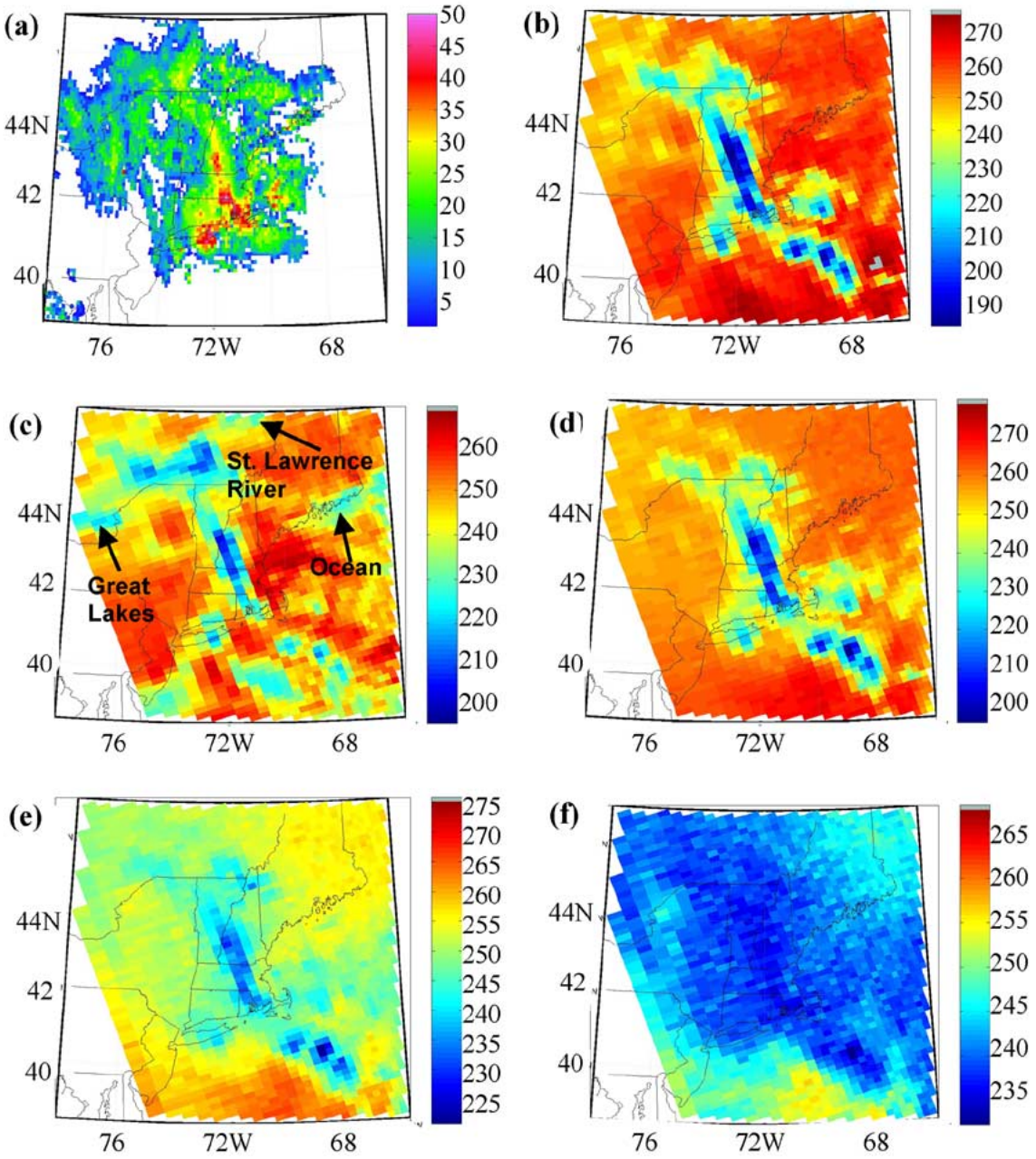

Fig. 1. (a) Radar reflectivity [logarithmic power (dBZ)] obtained from the NWS operational radar composite measured at 23:00 UTC March 5, 2001 and AMSU-B brightness temperatures observed 23:02 UTC March 5, 2001. (b) 150 GHz. (c) 89 GHz. (d) 183 $\pm$ 7 GHz. (e) 183 $\pm$ 3 GHz. (f) 183 $\pm$ 1 GHz.

expected that there are only three to four degrees of freedom in the five AMSU-B brightness temperature channels.

The first and second of the three variable parameters are used to adjust the distributions of the vertical structure of snow mass and relative humidity and are generated from the Pennsylvania State University–National Center for Atmospheric Research (PSU–NCAR) fifth-generation Mesoscale Model (MM5). During the retrieval, the parameterized snow model profile mass is allowed to extend beyond the confines of the MM5 simulations. This is necessary because the maximum surface snow mass over land produced by MM5 was only 0.8 g $\cdot$ m^{-3} corresponding to a lower reflectivity of 30 dBZ than seen in Fig. 1(a). Thus, the retrieved profiles are not just weighted combinations of the MM5 profiles, and they may vary more widely than the MM5 model profiles. The microphysical model of the falling snow also rests upon independent millimeter-wave attenuation measurements. The third adjustable parameter defines the fraction of snow ground cover and generates a composite surface emissivity using previously reported emissivities of snow and soil covered surfaces.

The three fixed parameters include height levels, temperature profiles, and snow size. The snow in the cloud profile is represented by equivalent spheres whose fixed diameters are of the same order of magnitude as those needed to model attenuation measured during previous field experiments. These parameters, along with the variable parameters, produce snow cloud characteristics used to generate a database of brightness temperatures that would be observed at the AMSU-B frequencies using for-

ward radiative transfer calculations. The optimal estimate of the snow parameters is derived from the best match between computed and measured brightness temperatures at *all* AMSU-B frequencies. Finally, the retrieved snowfall is compared to the radar reflectivity measurements provided by the NWS operational radars to estimate the validity of the retrieval.

A. MM5 Mesoscale Model

The MM5 model described by [11] and [12] was used in this study. A description of the MM5 model used here was presented by Chang *et al.* [13]. The model domain was centered at 35°N × 70°W; it consisted of 100 × 120 grid points with 40-km separation. The simulation generated profiles of temperature, relative humidity, cloud water, rain, cloud ice, snow, hail, and graupel mass at each of the grid points in the volume of the model domain.

The MM5 model was initialized at 00:00 UTC March 5, 2001, and model integration was performed for a period of 48 h. The initial and boundary conditions for the experiment were obtained by interpolating the National Center for Environmental Prediction (NCEP) $2.5° \times 2.5°$ global analysis for 00:00 UTC March 5, 2001 to the model grid points and then enhancing those with coincident rawinsonde soundings. The sea surface temperature data were also obtained from NCEP global analysis and were kept unchanged during the model integration. However, the land surface temperature was predicted using surface energy budget equations in which the effect of shortwave and longwave radiation and cloud radiation were included.

Any rain erroneously generated over coastal regions by the MM5 simulation was assumed to be snow because all of the reported temperatures in those areas were below −2 °C. The National Lightning Detection Network (NLDN) [14] observed some lightning off-shore, but *not* over New England. The cold land surface temperatures appeared unable to produce sufficient convection to produce lightning and perhaps graupel. Although not shown, the shape (but not the location) of the spatial distribution of precipitation over land and ocean from the MM5 model compares well with that of the radar reflectivity Z_{eff} shown in Fig. 1(a).

B. Snow Cloud Parameterization

Three fixed parameters in the retrieval include height levels, temperature profile, and spherical snow size. The height levels and temperature profiles were set to fixed values provided in Table I. The temperature profiles were determined by the average of the MM5 temperature profiles over land. The root mean square variability of the MM5 temperature profiles over land is minimal (about 10 K at lower altitudes). The three variable parameters and the fixed snow size will be described in detail in the following sections.

1) Relative Humidity Parameters: Profiles of the relative humidity with respect to ice used in the retrieval were modified by adding a scaled addition to a minimum relative humidity profile generated by the MM5 over land. Those profiles were interpolated between the values cited in Table I to yield

$$\text{RH}(z_i) = \text{RH}_{\min}(z_i) + \Delta\text{RH}(z_i)\mathbf{r} \tag{1}$$

TABLE I
ATMOSPHERIC PARAMETERS INFERRED FROM MM5 MODEL OF THE MARCH 5–6, 2001 BLIZZARD

Height (km)	T (K)	RH (%) $\text{RH}_{\min}$	RH (%) ΔRH	M(z), Normalized Snow Profile
0.02	267.50	80	20	1.00
0.5	267.13	70	30	0.95
1.0	266.75	60	40	0.90
2.0	266.27	20	80	0.76
3.0	265.23	11	89	0.61
4.0	261.72	9	91	0.51
5.0	255.77	6	94	0.35
6.0	248.64	4	96	0.20
8.0	232.51	2	98	0.06
10.0	221.37	2	98	0
12.0	222.52	2	34	0
14.0	220.94	2	18	0
16.0	216.61	2	16	0

where $\Delta\text{RH}(z_i) = \text{RH}_{\max}(z_i) - \text{RH}_{\min}(z_i)$ is the maximum range of acceptable relative humidity values from MM5, and z_i denotes the height at level i. The adjustable relative humidity scaling parameter $\mathbf{r}$ represents a single degree of freedom and ranges from 0.0–1.0 in 0.1 unit increments. The value of $\mathbf{r}$ was determined from the retrieval by minimizing the difference between observed and retrieval calculated brightness temperatures.

2) Surface Emissivity Parameter: The radiative transfer equation also requires knowledge of the emissivity of the variable surface features including accumulated snowfall. The boundary conditions were determined partially by the accumulated antecedent snow whose emissivities ε_s for deep dry snow at the relevant frequencies are obtained from [15]. Although [15] only measured emissivities to 150 GHz, they did provide curve fits for deep dry snow extending to 200 GHz. The 183-GHz emissivity was extracted from these curve fits. The values of ε_s at a 35° viewing angle are 0.64, 0.724, and 0.8 for 89, 150, and 183 GHz, respectively [15].

The emissivity used in the radiative transfer model is a weighted mean of the emissivity of snow cover ε_s and that of ε_o. The ε_o is an average of emissivities from bare soil, frozen soil, and winter forest/conifer and is 0.98 for all frequencies [16]. The effective emissivity is thus

$$\varepsilon = \mathbf{f}\varepsilon_s + (1 - \mathbf{f})\varepsilon_o \tag{2}$$

where $\mathbf{f}$ is the fraction of the ground covered by snow and has six values: 0.0, 0.2, 0.4,0.6, 0.8, and 1.0. The $\mathbf{f}$ parameter mostly af-

fects the 89-GHz brightness temperatures that permit the earth's surface to be seen through light precipitation.

3) Snow Mass Parameter: The snow mass for each profile layer is defined as the total mass of all snow particles in that layer. Representative snow mass profiles were taken from the MM5 snowing profiles over land and normalized with respect to their surface snow mass, to obtain a normalized profile $M(z)$ shown in Table I. Note that we consider the surface snow mass to be the snow mass at 20 m above the surface (see Table I). Since the MM5 snow profiles truncated to 0 g $\cdot$ m^{-3} at a 10-km height, the $M(z)$ profile has zero mass at a 10-km height (see Table I). Snow mass profiles used in the subsequent retrieval are scaled by a factor $\mathbf{m}$ in grams per cubic meter. The snow mass scaling parameter $\mathbf{m}$ can assume 39 values: 0.0, 0.02, 0.065, 0.1, 0.2, 0.4, 0.6, . . ., 6.8, 7.0 g $\cdot$ m^{-3}. These values convert to surface melted snowfall rates ranging from 0 to ~ 32 mm $\cdot$ h^{-1} or, equivalently, to reflectivities ranging from 0 to $\sim$48 dBZ. These snowfall rates, although beyond the land surface maximum of 0.8 g $\cdot$ m^{-3} given by the MM5 model, provide enough variability for the range of values in Fig. 1(a). The snow mass content profile used in the retrievals is

$$M_s(z_i) = \mathbf{m}M(z_i). \tag{3}$$

4) Snow Size Parameter Selection: The greatest challenge of snowfall studies is determining the electromagnetic properties of the wide variety of shapes and sizes of snowflakes. Microwave scattering and emission properties of hydrometeors depend on their size, shape, density, and whether they are frozen, melting, or liquid. Wet snow and sleet were reported along the New England coast, but the mean temperatures encountered in New Hampshire and Vermont remained around -5 °C, and reported maxima were only -2 °C. Furthermore, our case study observations are at 23:00 UTC or 19:00 local time when the temperatures are less than the daytime highs and retrievals are only performed over inland regions. Snow particles in this study were, therefore, regarded as dry containing no melt water.

We first assumed that the mass densities of the MM5 model consisted of large fluffy snow particle size distributions (i.e., 10% ice, 90% air) as suggested by Rutledge and Hobbs [17]. Effective medium mixing theories have been used by [5], [6], [18], and [19] to represent the dielectric constant of snow at frequencies below 90 GHz [20]. Using these models for the higher frequencies seemed to produce inappropriate electromagnetic characteristics. For example, the low density particles represented by effective medium mixing models did not provide enough scattering because the asymmetry factor was too large. The asymmetry factor is a function of the particle shape, size, temperature, and ice–air–water composition and determines the direction(s) of scattering from a hydrometeor. Large asymmetry factors increased forward scattering of the radiation from the warm lower layers so that computed brightness temperatures were too warm. Although the finite difference time domain method [21] can be used to compute the scattering characteristics of nonspherical particles at any frequency, the shape of the frozen crystal habit can only be crudely estimated, so that a simpler approach appears to be justified.

One such simpler approach is the procedure of Grenfell and Warren [22]. Grenfell and Warren (G–W) represented randomly oriented frozen particles as a concatenation of "equivalent" ice spheres whose effective diameter was determined by the ratio of the volume-to-surface-area (V/A)

$$D_{\text{eff}} = 6 \text{ V/A}. \tag{4}$$

The G–W procedure transforms inhomogeneous nonspherical (e.g., fluffy) ice particles into an ensemble of solid ice spheres; this greatly simplifies the determination of the scattering properties of the hydrometeors. Representing irregular particles as ensembles of equivalent spheres, has been used in the cirrus cloud infrared radiation modeling community and their properties have been analyzed in [23] and [24]. G–W demonstrated that equivalent spheres can adequately describe the transmittance and reflectance of diffuse infrared radiation through randomly oriented prisms. Moreover, [25] showed that the equivalent sphere approach accounts for the shape transition from needles to plates. It is noteworthy that such effective diameters are mainly determined by the *small* dimensions, i.e., the thickness of large disks or the diameters of long cylinders [22, eq. (3)] in G–W rather than the *maximum* dimensions that are most frequently measured.

The distributions of effective diameters D_{eff} (in millimeters) based on the G–W model were represented by a Gamma function of order 1

$$N(D_{\text{eff}}) = N_0 D_{\text{eff}} \exp(-\Lambda_{\text{GW}} D_{\text{eff}}). \tag{5}$$

The size distribution intercept parameter N_0 is related to the G–W slope parameter Λ_{GW} and the snow mass density M_s (grams per cubic meter) at each height z_i

$$M_s(z_i) = \frac{\pi \rho_{\text{GW}}}{6} \int_{\infty}^{0} N(D_{\text{eff}}) {D_{\text{eff}}}^3 dD_{\text{eff}} \tag{6}$$

where $\rho_{\text{GW}} = \rho_{\text{ice}} = 0.917$ g $\cdot$ m^{-3} so that

$$N_0 = \frac{M_s(z_i)\Lambda_{\text{GW}}^5}{4\pi\rho_{\text{GW}}}. \tag{7}$$

Note that the N_0 value, and hence the $N(D_{\text{eff}})$ expression, varies with differing snow masses at each height z_i, through (7). Also note that the number of "equivalent" spheres will be greater than the actual number of nonspherical scattering particles. The effective polydispersion diameter weighted over such a size distribution is

$$\langle D_{\text{eff}} \rangle = \frac{4}{\Lambda_{\text{GW}}}. \tag{8}$$

Once the G–W size distribution was specified, the effective diameter was determined by employing measurements obtained from other snow events to infer the attenuation coefficient (and hence $\langle D_{\text{eff}} \rangle$) of snow to use in the electromagnetic scattering model. The size parameter $\langle D_{\text{eff}} \rangle$ was derived by applying Mie theory to compute the extinction coefficient $k_{\text{Sext}}(\text{km}^{-1})$ of

snow as a function of frequency ν (gigahertz). The attenuation per mass is

$$A(\nu, M_s) = 10 \log_{10}(e) \frac{k_{\text{Sext}}}{M_s}. \tag{9}$$

Results of those calculations were compared to $A(\nu, M_s)$ measured for several winter seasons for frequencies between 96 and 225 GHz in [26] and [27]. Fig. 2 compares the attenuation per mass as a function of frequency measured during the samples with curves generated by Mie theory for $\langle D_{\text{eff}} \rangle$ values between 0.02 and 0.2 mm. It is well known that the crystal habit varies with height and that $\langle D_{\text{eff}} \rangle$ diminishes with height [4]. A simplification was invoked because it is difficult to justify the introduction of diverse shapes in the model in the absence of measurements. Thus, snow particles were assumed to be spherical and to be represented by

$$\begin{aligned} \langle D_{\text{eff}} \rangle &= 0.10 \text{ mm}, \quad \text{for } 0.0 < z < 0.5 \text{ km} \\ &= 0.06 \text{ mm}, \quad \text{for } 0.5 < z < 10.0 \text{ km}. \end{aligned} \tag{10}$$

These dimensions are characteristic of the small crystal dimensions, i.e., the thickness of plates or diameters of needles [28], [29]. Furthermore, the $\langle D_{\text{eff}} \rangle = 0.1$ mm below 0.5 km better matched the ground-based observations of Nemarich *et al.* [26] and Wallace [27], while the $\langle D_{\text{eff}} \rangle = 0.06$ mm above 0.5 km yielded brightness temperatures that best match the AMSU-B observations. In fact, Section IV-B will show that the 150- and 183-GHz brightness temperatures are especially sensitive to the small particles found at higher altitudes.

C. Radiative Transfer Model

The radiative transfer calculations are an integral part of the retrieval method since they are used to minimize the error between the observed and the calculated brightness temperatures. The radiative transfer model requires vertical profiles of pressure, temperature and humidity as well as cloud water and cloud ice and precipitation. These quantities were obtained from the snow cloud parameterization and they were introduced into the Mie theory model. Although the scattering by snow is nearly conservative, the actual albedos for single scattering that appear in the radiative transfer model were not, because those were determined by absorption mainly due to water vapor. The albedos for single scattering thus varied with height as the constituents varied.

The radiative transfer model used to compute brightness temperatures given a hydrometeor profile is the delta-Eddington model. Microwave radiances 35° off nadir were computed from a second-order Eddington approximation [10] with delta scaling [30] for plane-parallel clouds. This permitted the radiances to be calculated analytically by representing them by a series of Legendre polynomials truncated after the first order. Those radiances were then inserted into the source function of the transfer equation to compute the brightness temperatures. Smith *et al.* [31] showed that such an algorithm produced acceptable brightness temperatures at a 53.1° viewing angle, but that it yielded unacceptable errors

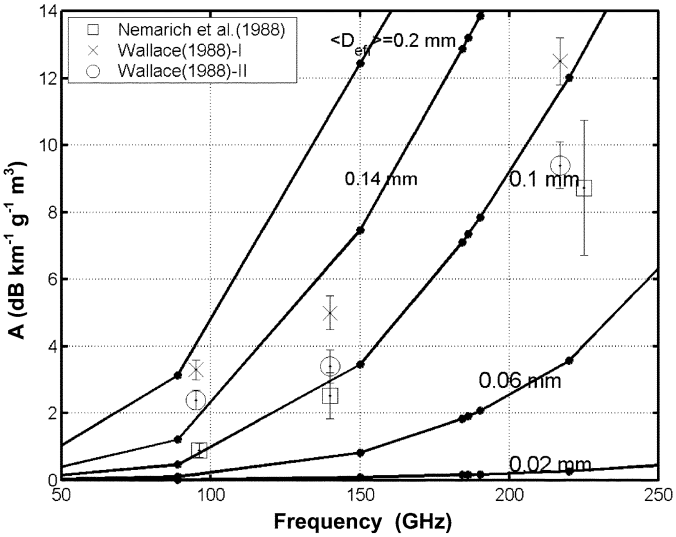

Fig. 2. Comparison between the attenuation per unit mass density ($\text{dB} \cdot \text{km}^{-1} \cdot \text{g}^{-1} \cdot \text{m}^3$) of snow versus frequency. Calculations (solid lines) are compared to various measurements in [27] and [26].

in brightness temperatures viewed at nadir. Accordingly the phase function (which mathematically describes the macroscopic direction and strength of the scattered radiation in each cloud layer) was approximated by representing the forward scattering component with a Dirac delta function in addition to a constant term and a term proportional to the cosine of the scattering angle. That procedure enabled both first *and* second moments of the approximate phase function to match those of a Henyey–Greenstein phase function. This model is identical to the previously cited Eddington second-order approximation except that the profiles of asymmetry factor, extinction coefficient and albedo for single scattering were scaled by transformed parameters. Smith *et al.* [31] and Kim *et al.* [32] showed that this transformation reduced the computational errors for both nadir and 53.1° viewing angles. We therefore assume that the radiative transfer model is valid for AMSU-B scanning angles between those limits.

D. Snowfall Retrieval

The parameters $\mathbf{r}$, $\mathbf{f}$, and $\mathbf{m}$ were found by an optimization that sought the minimum of

$$\Psi(\mathbf{r}, \mathbf{f}, \mathbf{m}) = \Sigma \left[\text{Tb}_j - \text{Tb}_j{}^o \right]^2 = \text{minimum} \tag{11}$$

where Tb_j and Tb_j^o are the computed and observed brightness temperatures for frequency j respectively, and the summation is over the five AMSU-B frequency channels. Since, for the current retrieval algorithm configuration, there are 11 $\mathbf{r}$, 6 $\mathbf{f}$, and 39 $\mathbf{m}$ values, the minimization occurs over the computed brightness temperature vectors associated with these 2574 potential cloud profiles. When additional information is acquired about the snow or other aspects of the storm, these can be included in (11) to further constrain the optimization. Furthermore, future versions of the retrieval algorithm will be modified for iterative optimization to allow any values of $\mathbf{r}$, $\mathbf{f}$, and $\mathbf{m}$ to be selected solely by (11).

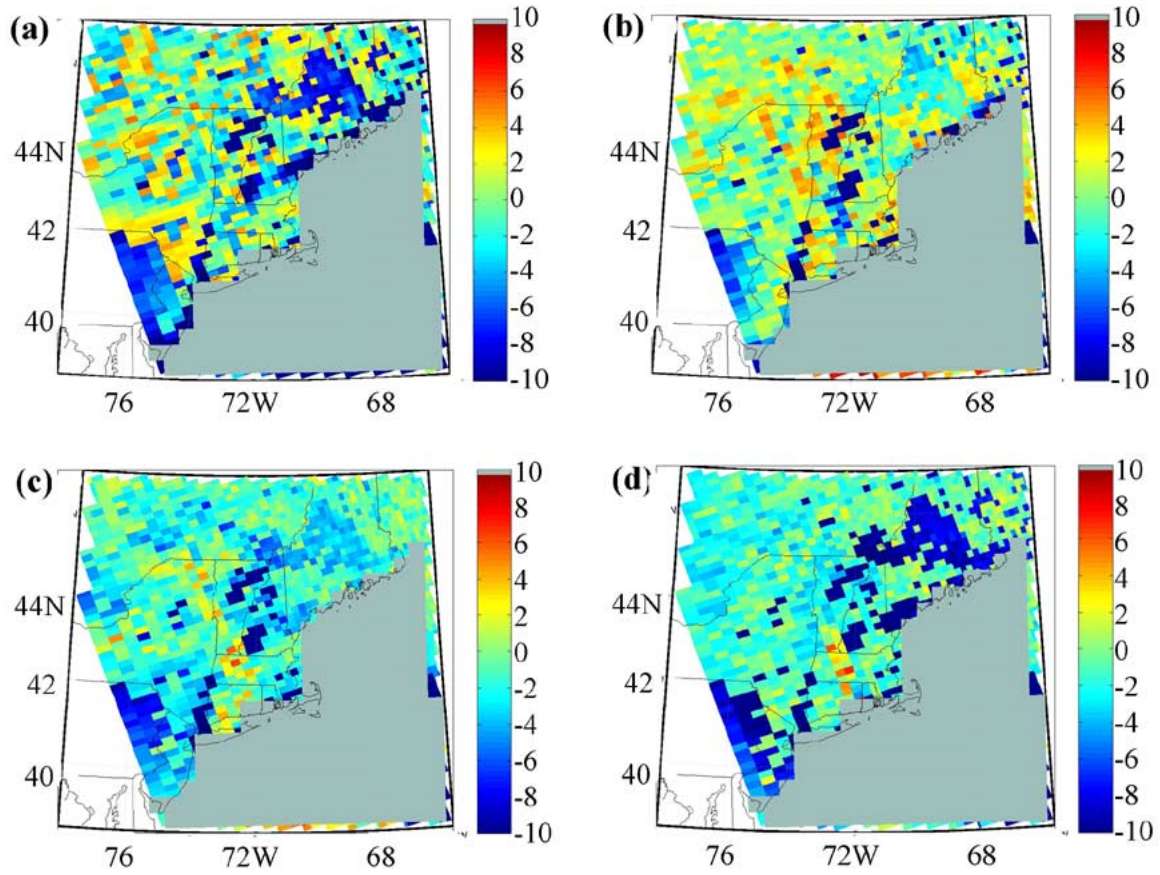

Fig. 3. Differences between optimized computed brightness temperatures and measured brightness temperatures at (a) 89, (b) 150, (c) 183 ± 7, and (d) 183 ± 3 GHz.

IV. Retrieval Results and Analysis

The retrieval was performed for the March 5–6, 2001 blizzard. The land surface temperature was assumed to be 267.5 K throughout the entire scene and the surface pressure was assumed to be 1010 mb. This surface temperature is a few degrees cooler than the reported inland daytime highs of -2 °C, since the local time of the AMSU-B observations was shortly after sunset. Fig. 3(a)–(d) illustrate the spatial distribution of brightness temperature errors that contributed to the $\Psi(\mathbf{r}, \mathbf{f}, \mathbf{m})$ residuals at 89, 150, and 183 ± 7, 3 GHz, respectively. Because this study is confined to the determination of snowfall over land, results over water are grayed out. The theoretical and experimental brightness temperatures agreed within approximately ± 5 K over most pixels at all of the AMSU-B frequencies; including 183 ± 1 GHz, which was not shown. The significance of the retrieved variables will be discussed in the following sections.

A. Retrieved Parameters

Fig. 4(a) shows the retrieved snowfall mass density near the surface, $M_s(0.02 \text{ km}) = \mathbf{m}\, M(0.02 \text{ km})$. It is evident that the spatial distribution of the snowfall mass is qualitatively similar to the radar reflectivity displayed in Fig. 1(a). Fig. 4(b) shows the distribution of the retrieved relative humidity at a 1-km altitude. The retrieved snow mass and relative humidity distributions are somewhat noisy. If more information were known about the profile (such as through vertical radar profiles and *in situ* measurements) it is expected that these variations would be reduced. Potential sources of this noise are discussed in Section IV-C.

Fig. 4(c) shows the distribution of the parameter $\mathbf{f}$, the fraction of snow cover on the ground within the AMSU-B field of view. Water in the Montreal, Quebec, and the St. Lawrence River regions (near 45° to 46°N, 73° to 76°W) may skew the retrieved snow cover fractions because the water surfaces have a lower emissivity than dry ground surfaces assumed in (2). The retrieval algorithm erroneously compensates for these lower emissivities (that produce cooler Tb) by increasing the snow fraction.

B. Weighting Functions

Temperature weighting vector profiles [33] can be used to understand contributions to brightness temperatures from each layer of the atmosphere, the cosmic background, and the ground. The brightness temperature at each frequency is the integrated sum over all heights of the product of the weighting vector value and the atmospheric temperature plus the contributions from the ground and cosmic background temperatures

$$Tb = \int_0^\infty T(z)W(z)dz = T_0 W_0 + T_{\text{CB}} W_{\text{CB}} + \sum_{i=1}^{I} T(z_i) W_{\text{ALL}}(z_i) \Delta z_i \quad (12)$$

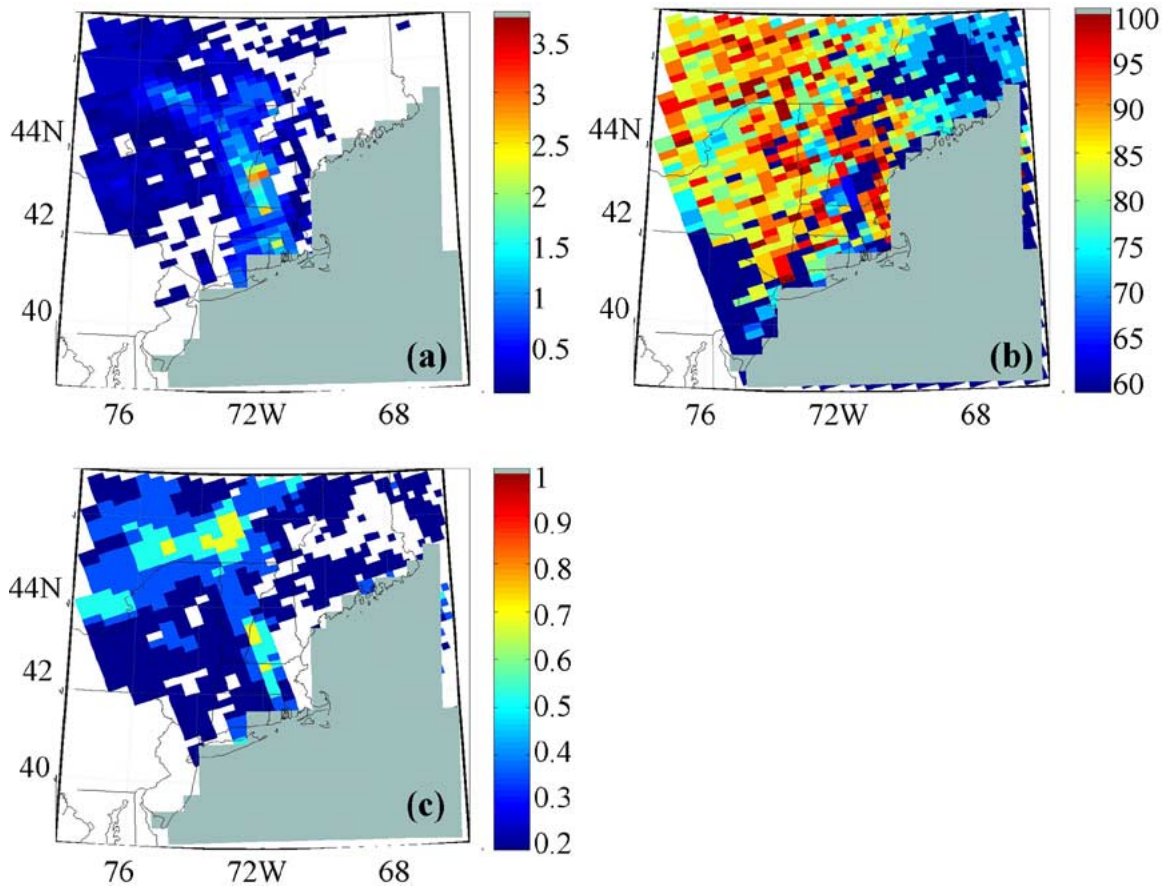

Fig. 4. Distribution of retrieved (a) snow mass at 20 m above the surface, (b) relative humidity at 1-km height, and (c) fractional snow cover.

where the subscripts 0 (at $z_i = 0$), and CB denote ground surface and cosmic background, respectively, $T(z_i)$, $W_{\rm ALL}(z_i)$ denote the temperature and weighting vector value, respectively, for level i of the cloud profile that consists of I levels, and Δz is the height increment between level i and level $i-1$. The weighting vectors depend on the profiles of the atmospheric cloud constituents and will change for various representative profiles. The weighting vectors $W_{\rm ALL}$, W_0, and $W_{\rm CB}$ are defined in [33] where $W_{\rm ALL}$ is denoted $W^{(n)}$.

The $W_{\rm ALL}$ includes the effects of multiple scattering by snow (S), and absorption by snow, water vapor (WV), nitrogen (N_2), and oxygen (O_2). In order to determine the contributions to the brightness temperature value from snow, water vapor, and other constituents, $W_{\rm ALL}(z_i)T(z_i)$ (with units of Kelvin per kilometer) at each z_i height is reorganized

$$W_{\rm ALL}(z_i)T(z_i) = M_S(z_i)W_S(z_i) + {\rm RH}(z_i)W_{\rm WV}(z_i) + W_{\rm other}(z_i)T(z_i). \quad (13)$$

We then define W_S, $W_{\rm WV}$, and $W_{\rm other}$ as

$$W_S(z_i) = \frac{k_{\rm Sext}(z_i)T(z_i)W_{\rm ALL}(z_i)}{k_{\rm ext}(z_i)M_S(z_i)}\ ({\rm K\cdot km^{-1}\cdot m^3\cdot g^{-1}}) \quad (14)$$

$$W_{\rm WV}(z_i) = \frac{k_{\rm WV}(z_i)T(z_i)W_{\rm ALL}(z_i)}{k_{\rm ext}(z_i){\rm RH}(z_i)}\ ({\rm K\cdot km^{-1}\cdot \%^{-1}}) \quad (15)$$

$$W_{\rm other}(z_i) = \frac{[k_{O2}(z_i)+k_{N2}(z_i)]\,W_{\rm ALL}(z_i)}{k_{\rm ext}(z_i)}\ ({\rm km^{-1}}) \quad (16)$$

where

$$k_{\rm ext}(z_i) = k_{\rm Sext}(z_i) + k_{\rm WV}(z_i) + k_{O2}(z_i) + k_{N2}(z_i). \quad (17)$$

The $k_{\rm Sext}$ term is the sum of the absorption and scattering coefficients for snow found in (9), $k_{\rm WV}$ is the absorption coefficient for water vapor, and k_{O2} and k_{N2} are the absorption coefficients for O_2, and N_2. Note that $k_{\rm ext}$ is also used in integrals within $W_{\rm ALL}$ as the atmospheric opacity. This means that W_S is not entirely free of the effects of the water vapor and other constituents, and likewise for $W_{\rm WV}$ and $W_{\rm other}$ however, they do respond to most of the information about the snow, water vapor, and other constituents, respectively.

In order to illustrate the physics of this retrieval, two representative retrieved profiles are studied. The first retrieved profile is extracted near the heaviest snowfall region, at 42.52°N, 72.036°W. The second profile at 40.77°N, 72.36°W is a lighter snowfall case and it is also much drier. For the first profile, (11) selects $\mathbf{r} = 0.7$, $\mathbf{m} = 2.6$ g $\cdot$ m^{-3}, and $\mathbf{f} = 0.8$ and for the second profile $\mathbf{r} = 0.3$, $\mathbf{m} = 0.6$ g $\cdot$ m^{-3}, and $\mathbf{f} = 0.4$. The retrieved snow and relative humidity profiles and surface emissivity can be computed using (1)–(3) and the profile information in Table I.

Table II compares the observed and computed brightness temperatures for these two representative retrieved profiles. This table shows fairly good agreement for all but the Profile 2 183 ±

TABLE II
BRIGHTNESS TEMPERATURE VALUES FOR TWO RETRIEVED PROFILES

	Profile 1	Profile 1	Profile 2	Profile 2
	AMSU-B	Retrieved	AMSU-B	Retrieved
89 GHz	209.2	206.5	233.9	232.0
150 GHz	185.5	185.7	221.4	219.5
183 ± 1 GHz	236.8	237.2	241.4	246.3
183 ± 3 GHz	234.1	232.9	244.3	247.4
183 ± 7 GHz	210.1	209.4	235.1	236.0

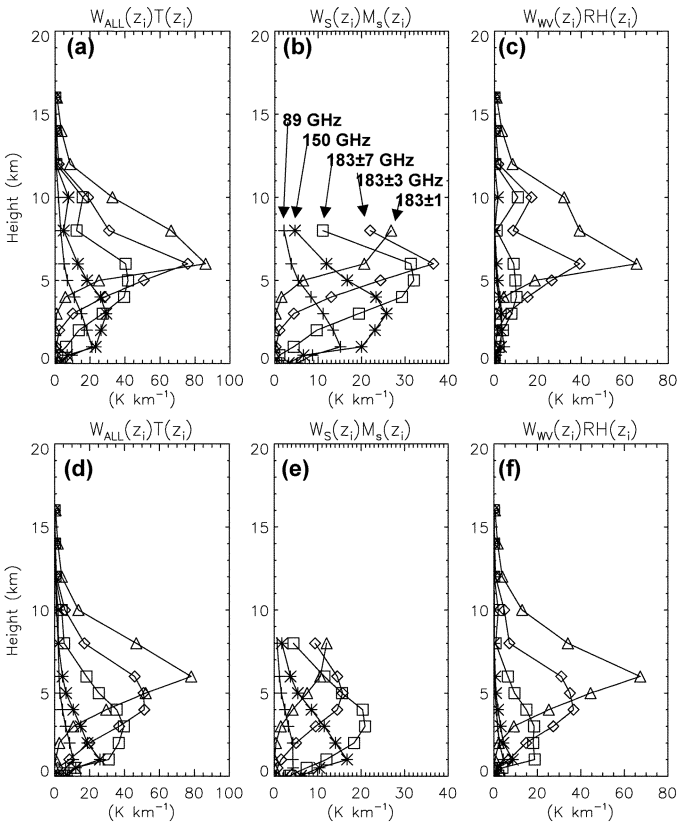

Fig. 5. Total (ALL), snow (S), and relative humidity (WV) weighting vectors of two sampled retrieved profiles. (a)–(c) Near the most intense snowfall region. (d)–(f) Near the storm boundary with low relative humidity.

1-GHz channel where there is a 5-K difference. This disagreement is likely due to a mismatch in the relative humidity for the second profile.

Plots of $W_{\rm ALL}(z_i)T(z_i)$, $W_S(z_i)M_s(z_i)$, and $W_{\rm WV}(z_i){\rm RH}(z_i)$ are shown in Fig. 5 for the two representative profiles. These plots can be used to determine the brightness temperature (by integrating over the heights and adding the cosmic background and surface contributions provided in Table III). The $W_{\rm WV}(z_i){\rm RH}(z_i)$ plots [Fig. 5(c) and (f)] show that the contribution of water vapor to the 183.3 $\pm$1- and $\pm$3-GHz brightness temperature is high at higher altitudes (above 5 km). For the other frequencies, the water vapor contribution is inversely correlated with the amount of snow in the cloud. By examining Fig. 5(b) and (e), it is noted that a decrease in $\mathbf{m}$ from 2.6 [Fig. 5(b)] to 0.6 g $\cdot$ m^{-3} [Fig. 5(e)] reduces the contribution from snow by nearly one half for all frequencies. Furthermore it should be noted that the 183-GHz channels respond to snow above the earth's surface, while the 89- and 150-GHz channels respond more intensely near the surface. The 89- and 150-GHz channels are also more sensitive to the surface emissivity, so some tradeoff must be made between the surface contributions and the snow contributions and contamination of the signal may occur. The 150-GHz channel is a little more immune to surface effects if the snow mass profile is large enough.

TABLE III
SURFACE AND COSMIC BACKGROUND BRIGHTNESS TEMPERATURE CONTRIBUTIONS (IN KELVIN) FOR TWO RETRIEVED PROFILES

	Profile 1	Profile 1	Profile 2	Profile 2
	T_0W_0	$T_{CB}W_{CB}$	T_0W_0	$T_{CB}W_{CB}$
89 GHz	111.8	0.5	180.8	0.37
150 GHz	25.7	0.8	110.9	0.5
183 ± 1 GHz	~0.0	0.1	0.01	0.06
183 ± 3 GHz	0.02	0.29	0.65	0.15
183 ± 7 GHz	1.4	0.55	16.4	0.33

The T_0W_0 in Table III show that the surface contribution from the 89-GHz channel is larger than that of the other channels and increases as we move from Profile 1 to Profile 2. In fact, the surface contributes at least half of the value of the resulting brightness temperatures for 89 GHz. A similar effect is seen for the 150-GHz surface weighting values, though heavy snow will obscure the surface for 150 GHz (Profile 1). The 183-GHz channels receive very little of their resultant brightness temperature values from the surface. All of the cosmic background contributions, $T_{\rm CB}W_{\rm CB}$, are small.

C. Radar Reflectivity Versus Melted Snowfall Rain Rate

A pixel area matching technique similar to that described in [34] was used to relate the radar reflectivity $Z_{\rm eff}$ (mm$^6 \cdot$ m^{-3}) derived from the dBZ$_{\rm eff}$ over land shown in Fig. 1(a) to the retrieved snowfall mass distribution, $M_s(0.02$ km) shown in Fig. 4(a). The procedure selected a number of pixels that exceeded a given snowfall mass and the same number of pixels that exceeded a particular radar reflectivity. Threshold values of each of these quantities were tabulated. The terminal velocity of snowflakes was assumed to be ~ 1 ms^{-1} so that the melted snowfall rates, R(mm $\cdot$ h^{-1}), could be derived by multiplying $M_s(0.02$ km) by that terminal velocity.

Fig. 6 presents dBZ$_{\rm eff}$ as a function of $\log(R)$ derived from this pixel matching technique for the retrieval results reported in Fig. 4. These results are compared to representative $Z_{\rm eff}$–R relationships [35]–[38] that showed the coefficients of snow $Z_{\rm eff}$–R relationships could vary over a wide range. The coefficients in such $Z_{\rm eff}$–R relationships have been refined over the years as snow measuring techniques have become more sophisticated. The comparison of the retrieved relationship to some previously published relationships is surprisingly good. While this is not a

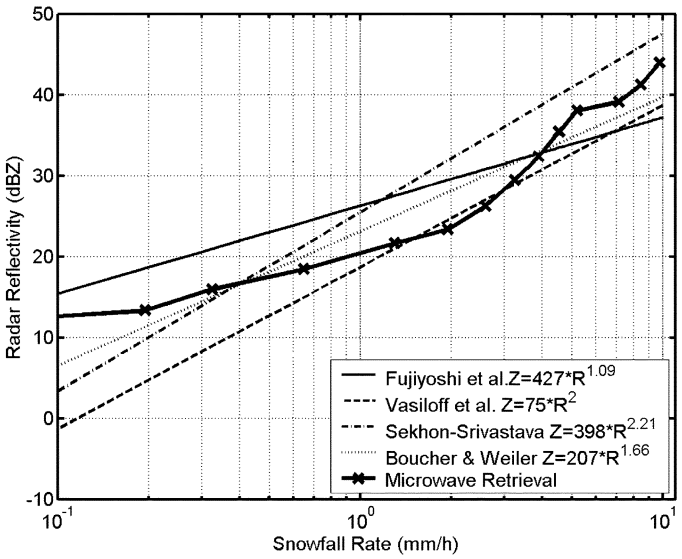

Fig. 6. Measured NWS radar reflectivity Z versus melted snowfall rate R (mm $\cdot$ h^{-1}) inferred from the $M_s(0)$. Results are compared to Z–R relationships found in [34]–[37].

direct validation of the retrieval results, it does show that this physical model enables retrievals to fall within existing measured and empirical relationship bounds.

D. Error Discussion

Because there are only three to four degrees of freedom associated with the AMSU-B channels and few additional measurements to further constrain the retrievals, the number of parameters retrieved is limited. With a limited retrieved parameter set, assumptions were made about the vertical structure of the snow cloud, including fixed vertical profiles of temperature, water vapor, and snow mass shape. Unfortunately, these assumed profiles, taken from the MM5 cloud model simulations, could not be validated by *in situ* observations. Further constraints were made on the allowed variability of the snow particle characteristics, by keeping the snow particle effective diameter relatively fixed throughout the profiles (but allowing the number of particles and the snow mass index $\mathbf{m}$ to vary).

Determining the electromagnetic (scattering, absorption, and asymmetry) properties of the snow leads to additional assumptions. The ones used herein include assuming: 1) dry snow; 2) that the Grenfell and Warren [22] approach to redistributing low-density fluffy snow into small ice spheres is appropriate; and 3) that the snow attenuation measured in [26] and [27] is similar to the retrieved case with a minor modification of the particle size. Fig. 2 showed that the attenuation of the particles assuming the G–W approach is relatively consistent with independently measured attenuation of snowfall. Other research [3], [39] on anvil ice particles and snowfall has shown that the retrieved particles sizes can be smaller than expected, giving credence to the applicability of the Grenfell and Warren approach. A detailed future analysis should include *in situ* sampling of snow particles that simultaneously determines size distributions and electromagnetic characteristics.

The noise in the retrieved snow mass, relative humidity indexes, and surface emissivity may be attributed to some of the assumptions made in this physically based retrieval:

1) selection of a single vertical shape $M(z)$ for the snow mass profiles [see 3)];
2) selecting a step function to describe the snow size distribution with height [see (10)];
3) assuming that equivalent spheres suffice to describe the electromagnetic properties of these frozen hydrometeors [see (4)–(7)];
4) assuming that the snow measured in [26] and [27] had the same habit as that at the surface in this New England blizzard;
5) ignoring frozen hydrometeors other than snow and assuming that snow was dry;
6) allowing the relative humidity index to vary independently of the snow mass index;
7) assuming that topography had no influence on the surface emissivity other than that represented by (2).

Another source of error and uncertainty is the conversion of the NOAA NWS composite data into reflectivities associated with snow falling near the ground. Radar validation of the melted snowfall rates retrieved from microwave brightness temperatures are fraught with large uncertainties both in terms of calibration of the operational NWS radars and the choice of the appropriate height from which measurements were blended to produce the mosaic of reflectivity values. While the reflectivities presented in summaries of operational NWS radars were not calibrated for research, they provide information about the intensity and horizontal structure of the storm. In the absence of a dedicated measurement campaign, the snowfall melted rain rates yielded a Z_{eff}–R relationship that was consistent with previous measurements.

V. Discussion and Conclusion

A physically based retrieval algorithm was developed to estimate snowfall over land. The retrieval algorithm relied on a multiparameter cloud model to generate the vertical structure of a snow cloud, including snow mass, snow particle effective diameter, and water vapor. The MM5 cloud simulation was used to provide useful statistics for generating those cloud characteristics. Ground-based attenuation measurements were used to characterize the equivalent sphere snow particle size used herein. The snow cloud profile and surface emissivity were then used in radiative transfer calculations that were optimized against AMSU-B observations at 89, 150, and 183.3 $\pm$ 7, $\pm$3, and $\pm$1 GHz. For each pixel in the image, the multiparameter cloud parameterization that produced brightness temperatures that best fit the AMSU-B observations was selected as the retrieved profile. This paper demonstrated the following.

1) Microwave radiometric channels operating at frequencies greater than 89 GHz provide information on snowfall over variable land surfaces because the surface emissivity is screened by water vapor absorption at those frequencies.
2) An electromagnetic scattering model of randomly oriented snow particles was adequately represented as equivalent spheres whose diameters were mainly determined by the small dimensions of the snow particles as suggested by Grenfell and Warren [22]. That model accounted for measured values of attenuation per unit

mass between 96 and 225 GHz. Inserting the G–W "equivalent" ice spheres in a delta-Eddington radiative transfer model yielded brightness temperatures at 89, 150, and $183 \pm 1, \pm 3, \pm 7$ GHz that were consistent with values measured by AMSU within $\pm \sim 5$ K. This was, in part, due to the fact that the diameters of the equivalent particles were small so that the asymmetry factor was also small (as might be expected from Rayleigh-like scattering). Small asymmetry factors reduce the transmission of snow layers, thereby achieving lower brightness temperatures than those produced by a low-density fluffy snow particle ice–air effective medium with larger asymmetry factors.

3) Weighting vectors illustrated the relationships between the physical properties of the clouds (snow and water vapor characteristics) and the resulting brightness temperatures.
4) Three variables used to adjust the snow mass, relative humidity, and surface emissivity were sufficient to estimate snowfall rates consistent with NWS radar reflectivity measurements and to yield a Z_{eff}–R relationship that was consistent with others reported in the literature.

The number of retrieved parameters was kept to a minimum because there are only three to four degrees of freedom in the five AMSU-B channels. This paper emphasizes the need for a dedicated set of coincident observations that include microwave as well as microphysics measurements. Field campaigns are needed to measure the high-frequency electromagnetic properties of snow along with the habits of frozen hydrometeors to yield parameters that we were forced to derive from disparate observations. Such measurements need to include the *small* as well as the *large* dimensions of frozen hydrometeors. More realistic retrieval procedures can be developed when additional information becomes available.

ACKNOWLEDGMENT

The authors wish to thank R. Ferraro and H. Meng (NOAA) for providing NOAA 15 AMSU data, R. Houze (University of Washington) for insights regarding cloud physics, and D. Kitzmiller (NWS) for describing the procedures used to produce the NWS radar reflectivity composites. They also thank A. Lunsford (GST, NASA Goddard) for converting the NWS radar images into a quantitative data record. They are also grateful to T. Grenfell and S. Warren for valuable discussions regarding their work on IR scattering characteristics of ice particles. Interest in the work in this paper by R. Kakar (NASA HQ) and support from the Goddard Director's Discretionary Fund are also gratefully acknowledged. Finally, the authors thank the anonymous reviewers who provided thoughtful comments to improve this paper.

REFERENCES

[1] R. A. Houze, Jr., *Cloud Dynamics*. San Diego, CA: Academic, 1993.
[2] A. Chang and T. Koike, "Progress in AMSR snow algorithm development," in *Microwave Radiometry and Remote Sensing of the Earth's Surface and Atmosphere*, P. Pampaloni and S. Paloscia, Eds., 2000, pp. 515–523.
[3] J. A. Weinman and I. M. Hakkarinen, "Determination of maritime snowfall from radar and microwave radiometer measurements," in *Proc. AMS Conf. Cloud Physics*, San Francisco, CA, 1990.
[4] G. Liu and J. A. Curry, "Large-scale cloud features during January 1993 in the North Atlantic Ocean as determined from SSM/I and SSM/T2 observations," *J. Geophys. Res.*, vol. 101, pp. 7019–7031, 1996.
[5] J. L. Schols, J. A. Weinman, G. D. Alexander, R. E. Stewart, L. F. Angus, and A. C. Lee, "Microwave properties of frozen precipitation around a North Atlantic cyclone," *J. Appl. Meteorol.*, vol. 38, pp. 29–43, 1999.
[6] R. Bennartz and P. Bauer, "Sensitivity of microwave radiances at 85–183 GHz to precipitating ice particles.of precipitation to ice particle size distributions," *Radio Sci.*, vol. 38, no. 4, p. 8075, 2003. DOI: 10.1029/2002RS002626.
[7] C. Kongoli, P. Pellegrino, R. Ferraro, N. Grody, and H. Meng, "A new snowfall detection algorithm over land using measurements from the Advanced Microwave Sounding Unit (AMSU)," *Geophys. Res. Lett.*, vol. 30, no. 14, p. 1756, 2003. DOI:10.1029/2003GL017177.
[8] F. W. Chen and D. H. Staelin, "AIRS/AMSU/HSB precipitation estimates," *IEEE Trans. Geosci. Remote Sensing*, vol. 41, pp. 410–417, Feb. 2003.
[9] R. W. Saunders, T. J. Hewison, N. C. Atkinson, and S. J. Stringer, "The radiometric characterization of AMSU-B," *IEEE Trans. Microwave Theory Tech.*, vol. 43, pp. 760–771, Apr. 1995.
[10] J. A. Weinman and R. Davies, "Thermal microwave radiances from horizontally finite clouds of hydrometeors," *J. Geophys. Res.*, vol. 83, pp. 3099–3107, 1978.
[11] J. Dudhia, "A nonhydrostatic version of the Penn State-NCAR mesoscale model: Validation tests and simulation of an Atlantic cyclone and cold front," *Mon. Weather Rev.*, vol. 121, pp. 1493–1513, 1993.
[12] G. A. Grell, J. Dudhia, and D. R. Stauffer, "A description of the fifth-generation Penn State/NCAR Mesoscale Model (MM5)," Nat. Center Atmos. Res., Boulder, CO, NCAR Tech. Note NCAR/TN-398+STR, 1995.
[13] D. E. Chang, J. A. Weinman, C. A. Morales, and W. S. Olson, "The effect of spaceborne microwave and ground-based continuous lightning measurements on forecasts of the 1998 groundhog day storm," *Mon. Weather Rev.*, vol. 129, pp. 1809–1833, 2001.
[14] R. E. Orville and G. R. Huffines, "Cloud-to-ground lightning in the United States: NLDN results in the first decade 1989–98," *Mon. Weather Rev.*, vol. 129, pp. 1179–1193, 2001.
[15] T. J. Hewison and S. J. English, "Airborne retrievals of snow and ice surface emissivity at millimeter wavelengths," *IEEE Trans. Geosci. Remote Sens.*, vol. 37, pp. 1871–1879, July 1999.
[16] T. J. Hewison, "Airborne measurements of forest and agricultural and surface emissivity at millimeter wavelengths," *IEEE Trans. Geosci. Remote Sens.*, vol. 39, pp. 393–400, Feb. 2001.
[17] S. A. Rutledge and P. V. Hobbs, "The mesoscale and microscale structure of and organization of clouds and precipitation in mid-latitude clouds. Part XII: A diagnostic modeling study of precipitation in narrow cold frontal rainbands," *J. Atmos. Sci.*, vol. 41, pp. 2949–2972, 1984.
[18] C. F. Bohren and L. J. Battan, "Radar backscattering of microwaves by spongy ice particles," *J. Atmos. Sci.*, vol. 39, pp. 2623–2628, 1982.
[19] R. Meneghini and L. Liao, "Effective dielectric constants of mixed-phase hydrometeors," *J. Atmos. Oceanic Technol.*, vol. 17, no. 5, pp. 628–640, 2000.
[20] A. H. Sihvola, "Self-consistency aspects of dielectric mixing theories," *IEEE Trans. Geosci. Remote Sensing*, vol. 27, pp. 403–415, July 1989.
[21] C. Tang and K. Aydin, "Scattering from ice crystals at 94 and 220 GHz millimeter wave frequencies," *IEEE Trans. Geosci. Remote Sensing*, vol. 35, pp. 93–99, Jan. 1995.
[22] T. C. Grenfell and S. G. Warren, "Representation of a nonspherical ice particle by a collection of independent spheres for scattering and absorption of radiation," *J. Geophys. Res.*, vol. 104, 1999.
[23] J. S. Foot, "Some observations of the optical properties of clouds, Part II, Cirrus," *Q. J. R. Meteorol. Soc.*, vol. 114, pp. 145–164, 1988.
[24] Q. Fu, "An accurate parametrization of the solar radiative properties of cirrus clouds for climate models," *J. Climate*, vol. 9, pp. 2058–2082, 1996.
[25] S. P. Neshyba, T. C. Grenfell, and S. G. Warren, "Representation of a hexagonal ice crystal by a collection of independent spheres for scattering and absorption of radiation," in *Proc. 11th Conf. Atmospheric Radiation*, Ogden, UT, June 3–7, 2002, Paper JP3.
[26] J. Nemarich, R. J. Wellman, and J. Lacombe, "Backscatter and attenuation by falling snow and rain at 96, 140 and 225 GHz," *IEEE Trans. Geosci. Remote Sensing*, vol. 26, pp. 319–329, July 1988.
[27] H. B. Wallace, "Millimeter-wave propagation measurements at the ballistic research laboratory," *IEEE Trans. Geosci. Remote Sensing*, vol. 26, pp. 253–258, May 1988.

[28] A. H. Auer, Jr. and D. L. Veal, "The dimensions of ice crystals in natural clouds," *J. Atmos. Sci.*, vol. 27, pp. 919–926, 1970.
[29] P. V. Hobbs, S. Chang, and J. D. Locatelli, "The dimensions and aggregation of ice crystals in natural clouds," *J. Geophys. Res.*, vol. 79, pp. 2199–2206, 1974.
[30] G. E. Thomas and J. Stamnes, *Radiative Transfer in the Atmosphere and Ocean*. Cambridge, U.K.: Cambridge Univ. Press, 1999.
[31] E. A. Smith, P. Bauer, F. S. Marzano, C. D. Kummerow, D. McKague, A. Mugnai, and G. Panegrossi, "Intercomparison of microwave radiative transfer models for precipitating clouds," *IEEE Trans. Geosci. Remote Sensing*, vol. 40, pp. 541–549, Ma. 2002.
[32] M. J. Kim, G. M. Skofronick-Jackson, and J. A. Weinman, "Intercomparison of millimeter-wave radiative transfer models," in *Proc. IGARSS*, Toulouse, France, July 21–25, 2003.
[33] A. J. Gasiewski, "Microwave radiative transfer in hydrometeors," in *Atmospheric Remote Sensing by Microwave Radiometry*, M. A. Janssen, Ed. New York: Wiley, 1993, pp. 91–144.
[34] R. V. Calheiros and I. Zawadski, "Reflectivity-rain rate relationship for radar hydrology in Brazil," *J. Climate Appl. Meteorol.*, vol. 26, pp. 118–132, 1987.
[35] Y. Fujiyoshi, T. Endoh, T. Yamada, K. Tsuboki, Y. Tachibana, and G. Wakahama, "Determination of a Z-R relationship for snowfall using a radar and high sensitivity snow gauges," *J. Appl. Meteorol.*, vol. 29, pp. 147–152, 1990.
[36] S. Vasiloff, R. M. Rasmussen, M. Dixon, and F. Hage, "Evaluation of snow forecasts provided by the Weather Support DeIcing Decision Making (WSDDM) system," in *Proc. 9th Conf. Aviation, Range Aerospace Meteorology*, Orlando, FL, 2000, pp. 547–550.
[37] R. S. Sekhon and R. C. Srivastava, "Snow size spectra and radar reflectivity," *J. Atmos. Sci.*, vol. 28, pp. 944–983, 1970.
[38] R. J. Boucher and J. G. Weiler, "Radar determination of snowfall rate and accumulation," *J. Climate Appl. Meteorol.*, vol. 24, pp. 68–73, 1985.
[39] G. M. Skofronick-Jackson, J. R. Wang, G. M. Heymsfield, R. Hood, W. Manning, R. Meneghini, and J. A. Weinman, "Combined radiometer-radar microphysical profile estimations with emphasis on high-frequency brightness temperature observations," *J. Appl. Meteorol.*, vol. 42, no. 4, pp. 476–487, 2003.

Gail M. Skofronick-Jackson (S'84–M'97–SM'03) received the B.S. degree in electrical engineering from Florida State University, Tallahassee, in 1986, and the M.S.E.E. and Ph.D. degrees from the Georgia Institute of Technology, Atlanta, in 1988 and 1997, respectively.

From 1988 to 1990, she was an Associate Research Engineer with BellSouth Services, Atlanta, GA. She returned to the Georgia Institute of Technology in 1990 as a Graduate Research Assistant. In 1997, she joined the Universities Space Research Association as part of the Goddard Visiting Scientist Program, NASA Goddard Space Flight Center, and in 2000, joined the University of Maryland, Baltimore County, Goddard Earth Science and Technology Center. She is currently with the Microwave Sensors Branch, NASA Goddard Space Flight Center, Greenbelt, MD. Her research interests include passive remote sensing, radiative transfer theory, and microphysical cloud profile modeling and retrievals.

Dr. Skofronick-Jackson is a member of the American Meteorological Society and the American Geophysical Union.

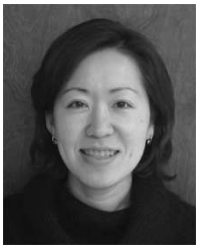

Min-Jeong Kim (S'03) received the B.S. degree in atmospheric sciences with a minor in physics from the Pusan National University, Pusan, Korea, and the M.S. degree in atmospheric sciences from the Seoul National University, Seoul, Korea, in 1995 and 1997, respectively. She is currently pursuing the Ph.D. degree at the University of Washington, Seattle.

Her studies have focused on numerical model simulations of air flow, cloud microphysics, and orographic precipitation caused by the complex topography of the Korean Peninsula. During her Ph.D. studies, she has worked on radiative transfer processes and microwave remote sensing of rainfall over the ocean, and since 2002, she has been studying the electromagnetic characteristics of frozen hydrometeors. She is currently developing a physical algorithm to retrieve snowfall over land, employing spaceborne millimeter-wave radiometers.

James A. Weinman (M'82–SM'98) received the Ph.D. degree in physics from the University of Wisconsin, Madison.

He is currently a Research Professor in the Atmospheric Science Department, University of Washington, Seattle. He was previously with the Microwave Sensing Branch, Goddard Space Flight Center, Greenbelt, MD, where he served as Branch Head for a limited period. Before joining NASA, he was a member of the faculty of the Meteorology Department, University of Wisconsin, Madison, from which he retired as Emeritus Professor. His research interests have included microwave remote sensing of precipitation, long-range measurements of VLF sferics, radiative transfer of solar and infrared radiation in horizontally inhomogeneous clouds, cloud morphology, and lidar propagation in turbid atmospheres.

Dr. Weinman is a Fellow of the American Meteorological Society and the Explorers' Club. He received the American Institute for Aeronautics and Astronautics Losey Award for studies on radiative transfer in the atmosphere and was awarded an Antarctic Service Medal for his participation in the International Geophysical Year.

Dong-Eon Chang received the B.S., M.S., and Ph.D. degrees in atmospheric sciences from Seoul National University, Seoul, Korea, in 1987, 1989, and 1998, respectively.

From 1990 to 1993, he served with the Republic of Korea Air Forces as a Forecast Officer. He returned to the Seoul National University in 1993 as a Graduate Research Assistant. In 1998, he joined the Universities Space Research Association as part of the Goddard Visiting Scientist Program, NASA Goddard Space Flight Center. He is currently with the Korea Meteorological Administration, Meteorological Research Institute, Seoul, since 2001. His research interests include mesoscale modeling and satellite data assimilation.

Dr. Chang is a member of the American Meteorological Society and the Korea Meteorological Society.